RSC Advances

ROYAL SOCIETY OF CHEMISTRY

www.rsc.org/advances

Graphical Abstract

Metal ionic size directed complexation in manganese(II) coordination chemistry: Efficient candidates showing phenoxazinone synthase mimicking activity

Anangamohan Panja

Influence of ionic size of metal on the diverse coordination chemistry of manganese(II) has been examined by the X-ray diffraction and IR spectral studies. Their relative phenoxazinone synthase activity has also been explored.

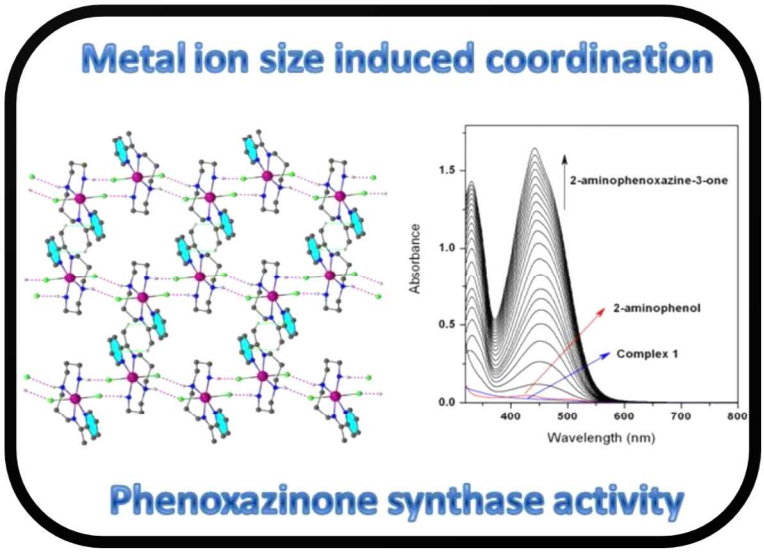

Metal ionic size directed complexation in manganese(II) coordination chemistry: Efficient candidates showing phenoxazinone synthase mimicking activity

Anangamohan Panja[*,a]

[a] *Postgraduate Department of Chemistry, Panskura Banamali College, Panskura RS, Purba Medinipur, West Bengal 721 152, India*

E-mail: ampanja@yahoo.co.in

ABSTRACT

The present report describes the syntheses and structural characterizations of two new mononuclear manganese(II) complexes, $[Mn(L^1)Cl_2]\cdot 2MeOH$ (**1**) and $[Mn(L^2)Cl_2]$ (**2**), in which L^1 and L^2 are tetradented ligands. Although the previous studies described that ligand L^1 exclusively binds the metal centers (Fe^{2+}, Ni^{2+} and Zn^{2+}) in the acyclic isomeric form (Schiff dibasic) of the ligand but in the present investigation it selectively binds Mn^{2+} ion through the cyclic (hexahydropyrimidine) analogue during complexation reaction as evidenced by the X-ray crystallography. The structure of **2** is quite interesting as it shows that one arm of Schiff dibasic form of the ligand has been hydrolyzed, suggesting that this type of ligands with Schiff dibasic form are incapable to yield the stable manganese(II) complexes. The metal ionic size directed hydrolysis of one arm of the ligand has been confirmed by IR spectral studies. Both the complexes are reactive towards the oxidation of *o*-aminophenol (OAPH), and their relative catalytic efficiency can nicely be explained by considering the steric contribution from the ligands and the electrochemical responses of

the metal center. From the experimental results a nice correlation, easily oxidizable metal center in the complexes showing higher catalytic activity, can be established between $E_{1/2}$ values and the catalytic activity. The kinetics study exhibited a deuterium kinetic isotope effect in the catalytic oxidative coupling of two moles of OAPH by O_2 as evidenced by the 1.6 times rate retardation in the deuterated solvent, suggesting to hydrogen atom transfer in the rate-determining step from the substrate hydroxy group to the metal-bound superoxo species.

Introduction

Schiff-base complexes those contain a carbon-nitrogen double bond have been extensively studied in the coordination chemistry mainly due to their ease of synthesis, tremendous structural diversities, and enormous possibilities towards various applications including catalysis.[1–3] In addition, they can easily undergo reversible reactions under certain conditions such as E−Z isomerization reactions, nucleophilic additions, transamination reactions, tautomerism, and aza Diels-Alder reactions. Among these, the condensation reactions of aromatic aldehydes with α,ω-di-primarypolyamines those contain both the primary and secondary amines are known to afford both Schiff dibases and their isomers with saturated heterocyclic rings (imidazolidine or hexahydropyrimidine).[4,5] Isomerization among these products through formation or opening of the heterocyclic ring in the presence of metal ions is quite common, and two factors viz Lewis acidity and the size of the metal ions are mainly responsible in such isomerization processes.[6,7] Boča et al.[8,9] have concluded that the relative acidity of imine-C and metal centers ultimately decides in which direction the isomerization of the ligand will shift. For example, weak Lewis acids such as Fe^{2+}, Co^{2+}, and Cu^{2+} are incapable (or only partly capable) to opening the heterocyclic ring, whereas stronger Lewis acids (e.g., Fe^{3+} and Zn^{2+}) can readily do it in order to gain denticity of the ligands. In contrast, Tuchagues et al.[10] postulated that the size of the metal ion is the determining factor in shifting

the ligand equilibrium towards the tautomeric form most appropriate to each specific cation. For instance, low-spin Fe^{2+} has a small enough ionic radius (75 pm) to fit inside the pocket provided by the imine isomers, while the ionic radius of Ni^{2+} (83 pm) is probably too large for allowing coordination of the imine tautomer, and thus it stabilizes the cyclic analogue.

We are working on the transition-metal complexes with pyridine containing ligands in order to develop functional mimics of various oxidase (oxygenase) metalloenzymes.[11–15] These studies are helpful to get insight into the natural systems in which metalloenzymes facilitate the spin-forbidden interaction between dioxygen and organic matter in the various biochemical reactions,[16–18] and ultimately provide clue for the development of bioinspired catalysts for the oxidation reactions in the industrial and synthetic processes. Our recent reports revealed that cobalt complexes with pyridine containing ligands are good functional models for the phenoxazinone synthase irrespective of the oxidation state of cobalt.[14] This multicopper oxidase is found naturally in the bacterium *Streptomyces antibioticus* [19,20] and catalyzes the oxidative coupling of two molecules of a substituted *o*-aminophenol to the phenoxazinone chromophore in the final step for the biosynthesis of actinomycin D.[21] The later is used clinically for the treatment of Wilm's tumor, gestational choriocarcinoma, and other tumors in which phenoxazinone chromophore is recognized to inhibit DNA-dependent RNA synthesis by intercalation to DNA.[22,23] In addition to copper-based models, some functional models of other metal ions, e.g. Fe^{3+}, Mn^{2+} and $Co^{2/3+}$, have also been reported. [11–15, 24–31] Moreover, few structure-property correlations that were determined are not sufficiently wide but only applicable for a set of few compounds and therefore, phenoxazinone synthase activity of new systems should be explored to get better insight and more straightforward structure-property correlations.

Our recent reports disclosed that the cobalt ion exclusively shows selectivity towards the Schiff dibasic form of the ligands derived from the condensation of pyridine-2-aldehyde

with α,ω-di-primarypolyamines, and even this selectivity is found to be insensitive to the oxidation states of cobalt, while manganese(II) ion prefers to bind with their cyclic analogue.[14,15] Size of the manganese(II) ion is too large to fit inside the cavity provided by Schiff dibasic form the ligands thereby preferring the cyclic analogue, which is consistent with the proposition made by Tuchagues et al.[10] In order to check whether manganese(II) ion exclusively selects the cyclic isomer over its Schiff dibasic form, in the present endeavor, the coordination ability of manganese(II) ion has been tested with the ligands those derived from the condensation of a triamine with longer propylenic linkers and pyridine-2-aldehyde (or 2-acetylpyridine). Syntheses and structural characterizations of two new manganese(II) complexes, $[Mn(L^1)Cl_2]\cdot 2MeOH$ (**1**) and $[Mn(L^2)Cl_2]$ (**2**), have been reported in which L^1 and L^2 are tetradented ligands as depicted in Scheme 1. The phenoxazinone synthase-like activity and its detailed kinetic studies to evaluate various kinetic parameters including turnover number for both the complexes have also been described.

Experimental section

Materials and physical measurements

Chemicals such as pyridine-2-aldehyde, 2-acetylpyridine and 3,3′-iminobis(propylamine) (Aldrich), and manganese(II) chloride tetrahydrate and *o*-aminophenol (Merck, India) were of reagent grade and used without further purification. Solvents like methanol, CD_3OD and diethyl ether (Merck, India), were of analytical grade and used as received.

Elemental analyses for C, H and N were carried out using a PerkinElmer 240 elemental analyzer. The infrared spectra of the complexes in KBr pellets were recorded in the 400–4000 cm^{-1} range on a PerkinElmer Infrared spectrometer. Electronic absorption spectra were recorded using a PerkinElmer Lamda-35 spectrophotometer with a

1-cm-path-length quartz cell. Electrochemistry was performed on an EG&G Princeton Applied Research potentiostat model 263A with a conventional three electrode system using a Pt working electrode, Pt auxiliary electrode and Ag/AgCl reference electrode. Electrospray ionization mass (ESI-MS positive) spectra were recorded on a micromass Q-TOF mass spectrometer.

Synthesis of $[Mn(L^1)Cl_2]\cdot 2MeOH$ (1)

A mixture of pyridine-2-aldehyde (0.428g, 4.0 mmol) and 3,3′-iminobis(propylamine) (0.262g, 2.0 mmol) in 30 ml of methanol was heated to reflux for 30 min. To the resulting yellow solution a methanol solution of $MnCl_2\cdot 4H_2O$ (0.396g, 2 mmol) was added and the mixture was continued to reflux for 30 min. The solution was allowed to cool at room temperature, and upon addition of ether a pale-yellow powder separated out from the solution. The precipitate was collected by filtration, washed with methanol/ether, and air dried. Yield: 0.800 g (83%). Crops of pale-yellow crystals suitable for X-ray analysis were obtained from slow diffusion of ether into a methanolic solution of the complex. Anal. Calcd. $C_{19}H_{27}Cl_2MnN_5O_2$: C, 48.11 %; H, 6.25 %; N, 14.02 %. Found: C, 47.67 %; H, 6.00 %; N, 14.08 %. IR (KBr, cm^{-1}): 3348 br (ν_{N-H} & ν_{O-H}); 1646 s ($\nu_{C=N}$, imine); 1597 s ($\nu_{C=N}$, pyridine). A major peak was detected at m/z = 399.07 corresponding to $[Mn(L^1)Cl]^+$.

Synthesis of $[Mn(L^2)Cl_2]$ (2)

A similar synthetic methodology was applied using 2-acetylpyridine (0.488g, 4.0 mmol), 3,3′-iminobis(propylamine) (0.262g, 2.0 mmol) and $MnCl_2\cdot 4H_2O$ (0.396g, 2 mmol) as starting materials and led to 0.574 g (80%) of a pale-yellow precipitate. Crops of dark-yellow crystals suitable for X-ray analysis were obtained from slow diffusion of ether into a methanol solution of complex **2**. Anal. Calcd. $C_{13}H_{22}Cl_2MnN_4$: C, 43.35 %; H, 6.15 %; N, 15.55 %. Found: C, 43.37 %; H, 6.27 %; N, 15.38 %. IR (KBr, cm^{-1}): 3239

br (ν_{N-H}); 1645 s ($\nu_{C=N}$, imine); 1598 s ($\nu_{C=N}$, pyridine). A base peak was detected at m/z =324.09 corresponding to $[Mn(L^2)Cl]^+$.

X-ray crystallography

Single crystal X-ray diffraction data for complexes **1** and **2** were collected on a Bruker SMART APEX-II CCD diffractometer using graphite monochromated Mo-Kα radiation. The unit cell was determined from the setting angles of 36 frames of data. Several scans in φ and ω directions were made to increase the number of redundant reflections and were averaged during the refinement cycles. Data processing for both the complexes were performed using the Bruker Apex2 suite.[32] Reflections were then corrected for absorption, inter-frame scaling, and other systematic errors with SADABS.[32] All the structures were solved by the direct methods and all non-hydrogen atoms were refined by the full-matrix least squares based on F^2 using the SHELXL-97[33] program within the WINGX package.[34] Hydrogen atoms attached to carbon atoms were included in the structure factor calculation in geometrically idealized positions, while those connected to nitrogen and oxygen atoms were located in the difference Fourier maps. The hydrogen atoms were isotropically treated using a riding model with their isotropic displacement parameters depending on the parent atoms. Relevant crystallographic data together with refinement details for the complexes are given in Table 1.

Kinetics of the phenoxazinone synthase activity

In a typical experiment, complexes **1** or **2** were mixed with *o*-aminophenol (OAPH) in air-saturated methanol and the oxidation of OAPH was followed spectrophotometrically by monitoring the growth of the absorbance as a function of time at 435 nm ($\varepsilon = 24 \times 10^3$ M^{-1} cm^{-1}),[27] which is characteristic of 2-aminophenoxazin-3-one in methanol. To determine the dependence of rate of the reaction on substrate concentration and to evaluate

various kinetic parameters, 1×10^{-4} M solution of the complexes were treated with at least 10 equivalents of substrate so as to maintain the pseudo-first order condition. Similarly, varying amounts of the catalyst, $(5 - 100) \times 10^{-5}$ M, were mixed with a fixed concentration (1×10^{-2} M) of substrate in methanol (2.0 ml) saturated with dioxygen in order to examine the catalyst dependency on rate of the reaction. The initial rate method was applied to determine the rate of a reaction, and the average initial rate over three independent measurements was determined by linear regression from the slope of absorbance versus time plot.

Results and discussion

Syntheses and general characterizations

The condensation of a polyamine with pyridine-2-aldehyde in 1:2 molar ratio yields a mixture of Schiff dibase and its heterocyclic analogue, and the ratio of which can be examined by the NMR spectroscopy.[9,10,35] Recent reports revealed that the metal-assisted ring opening/closing processes are common for such ligand systems, and several factors are responsible in this isomerization process including size of the metal ions, Lewis acidity, and stereochemistry of the metal centers.[9,10,35] We have recently examined the coordination ability of manganese(II) ion with this class of ligands derived from the condensation of two different triamines with pyridine-2-aldehyde, and the results show the selective complexation ability of manganese(II) ion to the cyclic form of the ligands.[15] In order to explore whether the manganese(II) ion exclusively selects the cyclic isomeric form, in the present work, the ligands derived from the condensation of two equivalents of pyridine-2-aldehyde (or 2-acetylpyridine) and one equivalent of 3,3′-iminobis(propylamine) with two longer propylenic linkers were allowed to react with hydrated salt of manganese(II) chloride in methanol (Scheme 1). On the basis of

characterizations of the complexes including X-ray crystal structures (*vide infra*), they are formulated as $[Mn(L^1)Cl_2]\cdot 2MeOH$ (**1**) and $[Mn(L^2)Cl_2]$ (**2**). Complex **1** is usual as found in our recent report,[15] but complex **2** is quite different as one arm of the Schiff base has been hydrolyzed during course of the reaction (*vide infra*).

In the IR spectra of complex **2**, a medium intense peak at 3239 cm^{-1} indicates N−H stretching vibration of the ligand. But the N−H stretching band overlaps with the O–H stretching vibration of the lattice methanol molecules in **1**, and the resultant broad band was observed at 3348 cm^{-1}. In the IR spectra of both the complexes, a strong and sharp band due to azomethine ν(C=N) appeared at 1646 and 1645 cm^{-1}, respectively. In addition, sharp peaks were observed at 1597 and 1598 cm^{-1} for complexes **1** and **2**, respectively, which might be assigned to stretching vibration of pyridyl C=N bond.

Structural studies

Crystal structure of complex **1** along with atom numbering scheme is depicted in Fig. 1, and selected bond lengths and angles are given in Table 2. Complex **1** crystallizes in the monoclinic $P2_1/c$ space group with two lattice methanol molecules, one of which is disordered over a crystallographic inversion center. Although ligand L^1 possesses one chiral center but the centrosymmetric space group suggests that the compound crystallizes as racemates. The geometry of the metal center is a pseudo-octahedron comprised of two pyridyl, one amine (hexahydropyrimidine) and one imine nitrogen donors from the folded dissymmetric ligand L^1, and two exogenous chloride ions. In the crystal structure, both the folded dissymmetric pyridyl nitrogen atoms and two chloride ions are cis coordinated, and two pyridyl rings are approximately perpendicular to each other (dihedral angle 86.30°). The Mn–N_{py} [2.302(2) and 2.324 Å] and Mn–N_{imine} [2.302(2) Å) distances are very similar but somewhat shorter than Mn–N_{amine} [2.367(2) Å] distance, which is along with line of the state of hybridizations of nitrogen atoms. The Mn–Cl bond lengths are found to be 2.461(1)

and 2.467(1) Å, and all the bond lengths are comparable to the related complexes with similar environment.[35–39] The degree of distortion from the ideal octahedral geometry (90/180°) is reflected from both the *cisoid* and *transoid* angles as shown in Table 2. Such distortion from the ideal octahedral geometry is presumably due to the shorter bite angles of the dissymmetric ligands especially those forming five-membered chelate rings. Five-membered chelates involving imine-N are conjugated and have a nearly planar conformation as expected, while remaining one is in the envelope conformation indicating saturated non-planar characteristic. Moreover, the six-membered hexahydropyrimidine rings are in more stable chair conformation as found in most of the systems.[10] The secondary amine hydrogen atom of hexahydropyrimidine ring involves in the intramolecular hydrogen bonding with a coordinated Cl atom, dimension of which is given in Table 3. In addition, that secondary amine nitrogen atom forms hydrogen bond with ordered solvent methanol molecule in **1**. The disordered solvent methanol molecule, sitting on an inversion center, also engages in the hydrogen bonding with two adjacent ordered methanol molecules (Table 3). These hydrogen bonds together with the edge-to-edge π–π stacking interaction (3.422Å) lead to the formation of a 3D supramolecular network of **1** as shown in Fig. S1.

The crystal structure of compound **2** is presented in Fig. 2, and principal bond lengths and angles are listed in Table 2. Complex **2** crystallizes in the monoclinic *C*2/c space group in which complex molecule sits on a general position. The manganese(II) ion is in a distorted-octahedral environment, comprised of the four nitrogen atoms of the L^2 ligand in the equatorial plane, and two exogenous chloride anions in the apical positions. The Mn–Cl and Mn–N distances are similar to what is observed for manganese(II) complexes of similar coordination environments. Several bond angles in **2** (Table 2) deviate significantly from the ideal value of 90° or 180° characteristic of a regular octahedron. The crystal

packing of complex **2** is mainly stabilized by moderately strong hydrogen bonding interactions involving amine-H and coordinated Cl^- ions (Table 3), which lead to the construction of a supramolecular 1D chain propagating along the *b* axis (Fig. 3). These supramolecular chains are further interacted with each other by means of C–H···π stacking interaction (2.951Å) which results a 2D sheet in the *ab* plane.

Metal-catalyzed hydrolysis of imine bond

Crystal structure of complex **1** shows that the manganese(II) ion selects again the cyclic isomer for stability during the complexation process.[15] Tuchagues et al.[10] reported a number of complexes with different metal ions (Fe^{2+}, Ni^{2+} and Zn^{2+}) with three different ligand systems. They found that regardless of the metal ions the cyclic form of the ligand derived from a triamine with two shorter ethylinic linkers is stabilized through the tetra-coordination, while acyclic Schiff dibasic isomer of L^1 (derived from a triamine with two longer propylinic linkers) is stabilized through penta-coordination in order to gain extra stability by increasing the donor sites. Based on the observations, they concluded that size of the metal ions is determining factor over Lewis acidity for the stability of the different isomeric forms of the ligands in the complexation process. Unlike to their observation, the longer propylenic linkers of the present triamine (in L^1) is unable to stabilize the Schiff dibasic form of the ligand in the manganese(II) coordination compound. Ionic radios of Mn^{2+} is even larger than Fe^{2+}, Ni^{2+} and Zn^{2+} and thus Schiff dibasic form of ligand L^1 is unable to accommodate Mn^{2+} ion. This result is further strengthening the proposition made by Tuchagues and coworkers that critical role of size of the metal ions in yielding complexes with either the cyclic or acyclic isomer is the deciding factor. In order to further confirm whether the manganese(II) ion has any tendency to stabilize the Schiff dibasic form, similar experiment was carried out with the ligand derived from the

condensation of same triamine with 2-acetylpyridine which is expected to produce only the Schiff dibasic ligand because methyl substitution on the azomethine-C not only reduces the electrophilic character of the imine-C but also increases the steric hindrance to the approaching nucleophile. But the structural study of complex **2** indicates that one arm of the Schiff base has been hydrolyzed. In our recent report, we have shown that *in situ* condensation of 3,3′-iminobis(propylamine) and 2-acetylpyridine followed by the addition of cobalt(II) salt yielded a dinuclear cobalt(III) complex in which Schiff dibasic ligand was coordinated to the metal centers.[14] Solution IR spectral studies were carried out to check whether the complex **2** arising from the hydrolysis of one arm of the Schiff dibasic ligand instead of half condensation reaction of triamine and 2-acetylpyridine (1:1 condensation). The *in situ* prepared ligand derived from the condensation of 3,3′-iminobis(propylamine) and 2-acetylpyridine in 1:2 molar ratio did not show any stretching for keto group (Fig. 4). The absence of the stretching band for keto group and the appearance of stretching of azomethine group (at 1645 cm^{-1}) confirm the double condensation. Interestingly, upon addition of manganese(II) chloride, a new band appeared at 1697 cm^{-1} which is due to the free 2-acetylpyridine, and this observation supports the hydrolysis of one arm of the ligand during the complexation process. The present results firmly conclude that size of the manganese(II) ion is too large to allowing coordination of the Schiff dibasic form of the ligands especially those derived from triamines and pyridine-2-aldehyde (or 2-acetylpyridine).

Cyclic voltammetry

The transition metal-based enzymes catalyze the redox processes in the biochemical reactions in which the redox potential of the metal centers plays important role. Therefore, the electrochemical behaviors of their models are of profound importance that could give us clue to their catalytic ability. The electrochemical behavior of the complexes was

investigated in acetonitrile solution containing 0.1 M tetraethylammonium perchlorate (TEAP) as a supporting electrolyte. Cyclic voltammograms of complexes **1** and **2** are depicted in Fig. 5 and Fig S2, respectively, and the electrochemical data for both the complexes are summarized in Table 4. Scanning in the anodic direction reveals a reduction wave at 0.93 and 0.76 V for **1** and **2**, respectively, which is due to the oxidation of manganese(II) to manganese(III). Upon reversal of the scan direction, the resultant manganese(III) complex is reduced to manganese(II) at 0.75 and 0.61 V for **1** and **2**, respectively. These nearly quasi-reversible electrode responses for Mn(II)/Mn(III) oxidation process is in line with the closely related manganese(II) complexes of similar ligand environment.[15,39,40] $E_{1/2}$ value of 0.84 V for complex **1** is significantly higher than **2** (0.68 V) which might be due to the different electronic environments in these complexes. The higher σ donor ability of both the primary and secondary amine groups in L^2 pusses much more electron density towards the metal center favoring the oxidation of manganese(II) center in **2**.

Phenoxazinone synthase like activity

The reaction between *o*-aminophenol and dioxygen in the presence of catalytic amount of complexes **1** or **2** as catalysts was performed in dioxygen-saturated methanol because of the good solubility of the complexes, the substrate, and the final product in this solvent. In order to avoid the autoxidation of the substrate by air the catalytic activity was examined in the absence of an added base. Before going to the detailed kinetic investigation, it is necessary to check the ability of the complexes to behave as catalysts for the oxidation of *o*-aminophenol. For this purpose 1.0×10^{-4} M solutions of the complexes (**1** or **2**) were treated with a 0.01 M solution of OAPH, and the growth of the absorption band of the phenoxazinone chromophore at 435 nm as a function of time was observed, which indicates catalytic oxidation of *o*-aminophenol to the corresponding

2-aminophenoxazin-3-one. A representative time resolved spectral profile for a period of 2 h after the addition of OAPH for complex **1** is shown in Fig. 6. In order to establish the importance of metal-complex conclusively in the catalytic process, a control experiment was performed in which OAPH was treated only with ligand L^1 and time course data of the resulted solution was recorded at 435 nm which did not show any significant growth of absorbance (Fig S3). Upon addition of methanolic solution of complex **1** to the same solution, progressive increase in the peak intensity was noticed. These observation clearly conclude that the phenoxazinone synthase activity arises solely from the manganese(II) complexes.

In order to understand the degree of catalytic efficiency kinetic studies of both the complexes were performed at 25 °C. For this purpose, 1×10^{-4} M solutions of the complexes were treated with at least 10-fold concentrated substrate solution as that of the complex to maintain the pseudo-first-order condition. For a particular complex-substrate mixture, time scan at the maximum band of 2-aminophenoxazine-3-one was carried out for a period of 30 min, and initial rate was determined by linear regression from the slope of the absorbance versus time. The initial rate of the reactions verses concentration of the substrate plot shows rate saturation kinetics (Fig. 7). This observation indicates that 2-aminophenoxazine-3-one formation proceeds through a relatively stable intermediate, a complex-substrate adduct, followed by the redox decomposition of the intermediate at the rate determining step. The initial rates versus concentration of substrate data were then analyzed on the basis of the Michaelis-Menten approach of enzymatic kinetics to obtain the Lineweaver-Burk (double reciprocal) plot as well as values of the parameters V_{max}, K_M, and K_{cat}. The observed and simulated initial rates versus substrate concentration plots for **1** and **2** are depicted in Fig. 7, while the Lineweaver−Burk plots are displayed in Fig. 8. Analyses of the experimental data yielded Michaelis binding constant (K_M) value of (1.11 ±

0.08) × 10^{-2} M for **1** and (8.53 ± 1.05) × 10^{-3} (1.11 ± 0.08) × 10^{-2} M for **2**, V_{max} values of (6.54 ± 0.42) × 10^{-7} M^{-1} and (7.59 ± 0.64) × 10^{-7} for **1** and **2**, respectively. The turnover number (k_{cat}) value is obtained by dividing the V_{max} by the concentration of the complex used, and is found to be 23.54 and 27.32 h^{-1} for **1** and **2**, respectively. Moreover, for a particular substrate concentration, varying the complex concentration, a linear relationship for the initial rates was obtained, which shows a first-order dependence on the complex concentration (Fig. S4).

Comparative phenoxazinone synthase activity and probable mechanism

The reaction kinetics shows that both the complexes are very reactive towards the oxidation of *o*-aminophenol, and the rate saturation kinetics study clearly indicates that the reaction proceeds through the stable complex substrate intermediate formation. In order to justify the involvement of molecular dioxygen in the catalytic cycle, UV-vis spectra of a mixture of 1 × 10^{-4} M solution of complex **2** with 100 fold excess of OAPH were recorded in nitrogen atmosphere, and no spectral growth at 435 nm was observed until one hour of mixing. This observation unambiguously proves that molecular dioxygen oxidizes OAPH to the corresponding 2-aminophenoxazine-3-one in the catalytic cycle in the presence of manganese(II) complex as a catalyst. Based on the above results, a plausible mechanism is tempted involving stepwise pathways, keeping in mind that it is impossible to prove any single mechanism. A tentative catalytic cycle for the formation of the phenoxazinone chromophore is shown in Scheme 2. At the first step OAPH forms an adduct with the manganese(II) complex,[12,13] which yields an OAP radical by the reaction with molecular dioxygen in the rate determining step. The OAP radical may generate *o*-benzoquinone monoamine (BQMI) in many ways including oxidation by the manganese(III) center. Finally, 2-aminophenoxazine-3-one is produced via several oxidative dehydrogenation processes involving OAPH, O_2, and BQMI as shown in Scheme 2. In order to increase the

acceptability of the most probable mechanism, the mass spectral study of a 1:50 mixture of complex **1** and OAPH were recorded after 10 minutes of mixing in methanol (Fig. S5). The spectrum comprised of all the peaks that found for the complex alone, and these peaks at m/z = 31016, 363.09 and 399.07 are due to the mono-cationic species of $(L^1 + H)^+$, $[Mn^{II}(L^1) - H]^+$ and $[Mn^{II}(L^1)Cl]^+$ as indicated by the isotopic distribution pattern together with the line-to-line separation of 1.0. In addition, one minor peak at m/z = 472.15 is quite interesting because the peak position and line-to-line separation of unity clearly indicates that this peak arises due to 1:1 complex-substrate aggregate $[Mn^{II}(L^1)(OAP)]^+$ which is consistent with the rate saturation kinetics as discussed earlier. But the mass spectrum does not suggest any species related to dioxygen bound metal-complex. In our recent report, we have observed that the acyclic dibasic form of ligand L^1 yielded a peroxo-bridged dinuclear cobalt(III) complex and that compound exhibited phenoxazinone synthase activity.[14] Therefore, I speculated that in the present case dioxygen-bound metal center could play important role in the catalytic process. Whether manganese(III)-superoxo is the active species in abstracting the O–H proton of OAPH in the rate determining step, comparative kinetic studies were performed under a given set of conditions both in methanol and deuterated methanol. It can be assumed that in CH_3OD the phenolic–OH of OAPH undergoes nearly complete exchange for OD. Consequently, if the rate determining step involves in breaking of the –O–H (–O–D) bond, a kinetic isotope effect (KIE) should be observed upon going from CH_3OH to CH_3OD as solvent. In fact, 1.6 times rate retardation in the deuterated solvent suggests that hydrogen atom transfer in the rate-determining step from the substrate hydroxy group to the metal-bound superoxo species are operative in the catalytic oxidative coupling of two moles of OAPH by O_2.[28] However, the turnover numbers suggest that complex **2** is more reactive than **1** towards the phenoxazinone synthase activity. It has been well explored that the catalytic activity of a complex depends

on several factors such as geometry of the complex, redox potential of the central metal ion, and the steric factor. The present results can nicely be interpreted by considering the electrochemical potential in combination with the coordination environments around the metal center. Ligand L^2 in **2** is less bulky than L^1 in **1** and thus favors interaction of the substrate to the metal center. In addition, lower electrochemical response of complex **2** facilitates interaction of the metal center with molecular dioxygen in the catalytic cycle.

Conclusions

Two novel mononuclear manganese(II) complexes have been synthesized and structurally characterized by X-ray diffraction studies. Structural characterization reveals that the Mn^{2+} ion prefers the cyclic (hexahydropyrimidine) form of the ligand in **1** but in **2** one arm has been hydrolyzed during complexation reaction. It is already been reported that ligand L^1 exclusively binds the metal centers (Fe^{2+}, Ni^{2+} and Zn^{2+}) in the acyclic isomeric form of the ligand but higher ionic radius of Mn^{2+} ion enforces to stabilize the cyclic analogue during complexation. IR spectral results demonstrate that the size of manganese(II) ion is too large to allowing the coordination of the Schiff dibasic form of the ligands especially those derived from triamines and pyridine-2-aldehyde (or 2-acetylpyridine). The crystal packing of complex **2** is interesting as it forms 1D supramolecular chain through the hydrogen bonding interaction. Both the complexes are moderately active towards the oxidation of *o*-aminophenol, and their relative catalytic efficiency mainly arises from the steric contribution from the ligands and the electrochemical responses of the metal center. From the experimental results a nice correlation, easily oxidizable metal center in the complexes showing higher catalytic activity, can be established between $E_{1/2}$ values and the catalytic activity. The deuterium kinetic isotope effect in the catalytic oxidative coupling of two moles of OAPH by O_2 as evidenced by the 1.6 times rate retardation in the deuterated solvent unambiguously

suggests to hydrogen atom transfer in the rate-determining step from the substrate hydroxy group to the metal-bound superoxo species.

Acknowledgements

A. P. is grateful to the University Grants Commission, India for the financial support of this research (Sanction No. PSW-173/11-12). Jadavpur University and Indian Association for the Cultivation of Science, India, are also gratefully acknowledged for the instrumental facilities.

† Electronic supplementary information (ESI) available: The electronic supplementary information file contains Figs. S1–S5. CCDC 962739 and 997081 contain the supplementary crystallographic data for complexes **1** and **2**, respectively. For ESI and crystallographic data in CIF or other electronic format see DOI: To be filled by the publisher

References

1 E. Tsuchida and K. Oyaizu, *Coord. Chem. Rev*., 2003, **237**, 213–228.

2 L. Canali and D.C. Sherrington, *Chem. Soc. Rev*., 1999, **28**, 85–93.

3 J. Tisato, F. Refosco and F. Bandoli, *Coord. Chem. Rev*., 1994, **135**, 325–397.

4 R. J. Ferm and J. L. Riebsomer, *Chem. Rev*., 1954, *54*, 593–613.

5 R. J. Ferm, J. L. Riebsomer, E. L. Martin and G. H. Daub, *J. Org. Chem*., 1953, **18** 643–648.

6 M. Boca, D. Valigura and W. Linert, *Tetrahedron*, 2000, **56**, 441–446.

7 S. Deoghoria, S. Sain, M. Soler, W. T. Wong, G. Christou, S. K. Bera and S. K. Chandra, *Polyhedron*, 2003, **22**, 257–262.

8 M. Boca, P. Baran, R. Boca, G. Kickelbick, F. Renz and W. Linert, *Inorg. Chem. Commun*., 1999, **2**, 188–190.

9 M. Boca, P. Baran, R. Boca, M. Fuess, G. Kickelbick, W. Linert, F. Renz and I. Svoboda, *Inorg. Chem*., 2000, **39**, 3205–3012.

10 N. Bréfuel, C. Lepetit, S. Shova, F. Dahan and J.-P. Tuchagues, *Inorg. Chem*., 2005, **44**, 8916–8928.

11 A. Panja and P. Guionneau, *Dalton Trans*., 2013, **42**, 5068–5075.

12 A. Panja, M. Shyamal, A. Saha and T. K. Mandal, *Dalton Trans*., 2014, **43**, 5443–5452.

13 A. Panja, *Polyhedron*, 2014, http://dx.doi.org/10.1016/j.poly.2014.02.004.

14 A. Panja, *Dalton Trans*., 2014, 43, 7760–7770

15 A. Panja, *Polyhedron*, 2014, **79**, 258–268

16 E. I. Solomon, T. C. Brunold, M. I. Davis, J. N. Kemsley, S. K. Lee, N. Lehnert, F. Neese, A. J. Skulan, Y. S. Yang and J. Zhou, *Chem. Rev*., 2000, **100**, 235–349.

17 E. I. Solomon, R. Sarangi, J. S. Woertink, A. J. Augustine, J. Yoon and S. Ghosh, *Acc. Chem. Res*., 2007, **40**, 581–591.

18 E. G. Kovaleva and J. D. Lipscomb, *Nat. Chem. Biol*., 2008, **4**, 186–193.

19 C. E. Barry, P. G. Nayar and T. P. Begley, *Biochemistry*, 1989, **28**, 6323–6333.

20 A. W. Smith, A. Camara-Artigas, M. Wang, J. P. Allen and W. A. Francisco, *Biochemistry*, 2006, **45**, 4378–4387.

21 C. E. Barry, P. G. Nayar and T. P. Begley, *J. Am. Chem. Soc*., 1988, **110**, 3333–3342.

22 E. Frei, *Cancer Chemother. Rep*., 1974, **58**, 49–54.

23 U. Hollstein, *Chem. Rev*., 1974, **74**, 625–652.

24 L. I. Simándi, T. M. Simándi, Z. May and G. Bensenyei, *Coord. Chem. Rev*., 2003, **245**, 85–93.

25 M. Hassanein, M. Abdo, S. Gerges and S. El-Khalafy, *J. Mol. Catal. A*, 2008, **287**, 53–56.

26 R. Bakshi, R. Kumar and P. Mathur, *Catl. Commun*., 2012, **17**, 140–145.

27 C. Mukherjee, T. Weyhermuller, E. Bothe, E. Rentschler and P. Chaudhuri, *Inorg. Chem*. 2007, **46**, 9895–9905.

28 T. M. Simándi, L. I. Simándi, M. Győr, A. Rockenbauer and Á. Gömöry, *Dalton. Trans*., 2004, 1056–1060.

29 T. Horváth, J. Kaizer and G. Speier, *J. Mol. Catal. A*, 2004, **215**, 9–15.

30 J. Kaizer, G. Baráth, R. Csonka, G. Speier, L. Korecz, A. Rockenbauer and L. Párkányi, *J. Inorg. Biochem*., 2008, **102**, 773–780.

31 C. Mukherjee, T. Weyhermüller, E. Bothe and P. Chaudhuri, *C. R. Chimie*, 2007, 10, 313–325.

32 G. M. Sheldrick, *SAINT*, Version 6.02, *SADABS*, Version 2.03, Bruker AXS Inc., Madison, Wisconsin, 2002.

33 G. M. Sheldrick, *SHELXL97*, Program for Crystal Structure Refinement, University of Göttingen, Göttingen, Germany,1997.

34 L. J. Farrugia, *J. Appl. Crystallogr*., 1999, **32**, 837–838.

35 Y.-M. Lee, E.-S. Kim, H.-J. Kim, H. J. Choi, Y.-I. Kim, S. K. Kang and S.-N.Choi, *Dalton Trans*., 2009, 126–133.

36 S. E. Ghachtouli, A. Mohamadou and J.-P. Barbier, *Inorg. Chim. Acta*, 2005, 358, 3873–3880.

37 S. I. M. Paris, Ü. A. Laskay, S. Liang, O. Pavlyuk, S. Tschirschwitz, P. Lönnecke, M. C. McMills, G. P. Jackson, J. L. Petersen, E. Hey-Hawkins and M. P. Jensen, *Inorg. Chim. Acta*, 2010, 363, 3390–3398.

38 C. Hureau, S. Groni, R. Guillot, G. Blondin, C. Duboc and E. Anxolabéhère-Mallart.

Inorg. Chem., 2008, **47**, 9238–9247.

39 S. Groni, C. Hureau, R. Guillot, G. Blondin, G. Blainand and E. Anxolabéhère-Mallart, *Inorg. Chem*., 2008, **47**, 11783–11797.

40 C. Hureau, G. Blondin, M.-F. Charlot, C. Philouze, M. Nierlich, M. Césario and E. Anxolabéhère-Mallart, *Inorg. Chem*., 2005, **44**, 3669–3683.

Table 1. Crystal data and structure refinement for complexes **1** and **2**.

	1	**2**
Empirical formula	$C_{20}H_{31}Cl_2MnN_5O_2$	$C_{13}H_{22}Cl_2MnN_4$
Formula weight	499.34	360.19
Temperature (K)	293(2)	150(2)
Wavelength (Å)	0.71073	0.71073
Crystal system	Monoclinic	Monoclinic
Space group	$P2_1/c$	C2/c
a (Å)	10.4242(2)	19.2620(3)
b (Å)	9.1757(1)	11.7960(1)
c (Å)	24.4086(5)	17.1290(3)
β(°)	100.971(1)	122.207(5)
Volume ($Å^3$)	2292.00(7)	3293.09(20)
Z	4	8
D_{calc} (g cm^{-3})	1.401	1.453
μ (mm^{-1})	0.833	1.122
F(000)	1004	1496
θ range (°)	2.80 – 30.08	2.90 – 32.05
Limiting indices	$-14 \le h \le 14$,	$-28 \le h \le 28$,
	$-12 \le k \le 12$,	$-17 \le k \le 17$,
	$-33 \le l \le 34$	$-25 \le l \le 25$
Reflections collected	23831	10331
Independent reflection / R_{int}	6697 / 0.0592	5725 / 0.0159
Observed reelections	4739	5238
Data / restraints / parameters	6697 / 0 / 310	5725 / 0 / 185
Goodness-of-fit on F^2	1.043	1.071
Final *R* indices [$I>2\sigma(I)$]	R1 = 0.0482,	R1 = 0.0279,
	wR2 = 0.1286	wR2 = 0.0645
R indices (all data)	R1 = 0.0791,	R1 = 0.0279,
	wR2 = 0.1441	wR2 = 0.0710
Largest diff. peak / hole (e $Å^{-3}$)	0.881 / –0.766	0.514/ –0.528

Table 2. Selected bond lengths (Å) and bond angles (°) for **1** and **2**.

1

Mn1–N1	2.302(2)	Mn1–N5	2.324(2)
Mn1–N2	2.302(2)	Mn1–Cl1	2.4674(7)
Mn1–N3	2.367(2)	Mn1–Cl2	2.4620(7)
N1– Mn1–N2	71.69(7)	Cl1– Mn1–N1	89.80(5)
N1– Mn1–N3	158.37(8)	Cl1– Mn1–N2	160.94(6)
N1– Mn1–N5	93.63(8)	Cl1– Mn1–N3	105.41(6)
N2– Mn1–N3	91.35(8)	Cl1– Mn1–N5	90.46(6)
N2– Mn1–N5	86.30(8)	Cl2– Mn1–N1	98.19(5)
N3– Mn1–N5	71.38(8)	Cl2– Mn1–N2	86.74(6)
		Cl2– Mn1–N3	94.02(6)
		Cl2– Mn1–N5	163.64(6)
		Cl1– Mn1–Cl2	100.79(3)

2

Mn1–N1	2.2536(9)	Mn1–N4	2.2284(9)
Mn1–N2	2.2434(9)	Mn1–Cl1	2.5781(3)
Mn1–N3	2.2266(9)	Mn1–Cl2	2.5535(3)
N1– Mn1–N2	72.60(3)	Cl1– Mn1–N1	88.07(2)
N1– Mn1–N3	166.36(3)	Cl1– Mn1–N2	97.45(3)
N1– Mn1–N4	100.61(3)	Cl1– Mn1–N3	88.37(3)
N2– Mn1–N3	94.83(3)	Cl1– Mn1–N4	84.40(3)
N2– Mn1–N4	172.83(4)	Cl2– Mn1–N1	93.91(2)
N3– Mn1–N4	92.13(4)	Cl2– Mn1–N2	84.47(2)
		Cl2– Mn1–N3	90.02(3)
		Cl2– Mn1–N4	93.87(3)
		Cl1– Mn1–Cl2	177.58(1)

Table 3. Geometry of important hydrogen bonds (Å, º) for **1** and **2**.

	D–H···A	D–H	H···A	D···A	<D–H···A
1	O2–H1A···N4	0.82	2.03	2.836(5)	168
	O2–H2A···O1	0.93	1.98	2.842(13)	152
	N4–H4···Cl1	1.00	2.36	3.285(4)	154
2	N3–H3A···Cl1a	0.89	2.58	3.318(1)	140
	N4–H4B···Cl2b	0.90	2.47	3.357(1)	167

Symmetry code: a = 1/2–x, –1/2–y, –z; b = 1/2–x,1/2–y,–z

Table 4. Electrochemical data for **1**–**3** in acetonitrile [a]

Complex	E_p^c (V)	E_p^a (V)	ΔE_p (V)	$E_{1/2}$(V)
1	0.75	0.93	0.18	0.84
2	0.61	0.76	0.15	0.68

[a] Pt working and Ag/AgCl reference electrodes; supporting electrolyte tetraethylammonium perchlorate; Scan rate 100 mVs^{-1}; E_p^a and E_p^c are anodic and cathodic peak potentials respectively; $E_{1/2} = 0.5(E_p^a - E_p^c)$; $\Delta E_p = E_p^a - E_p^c$.

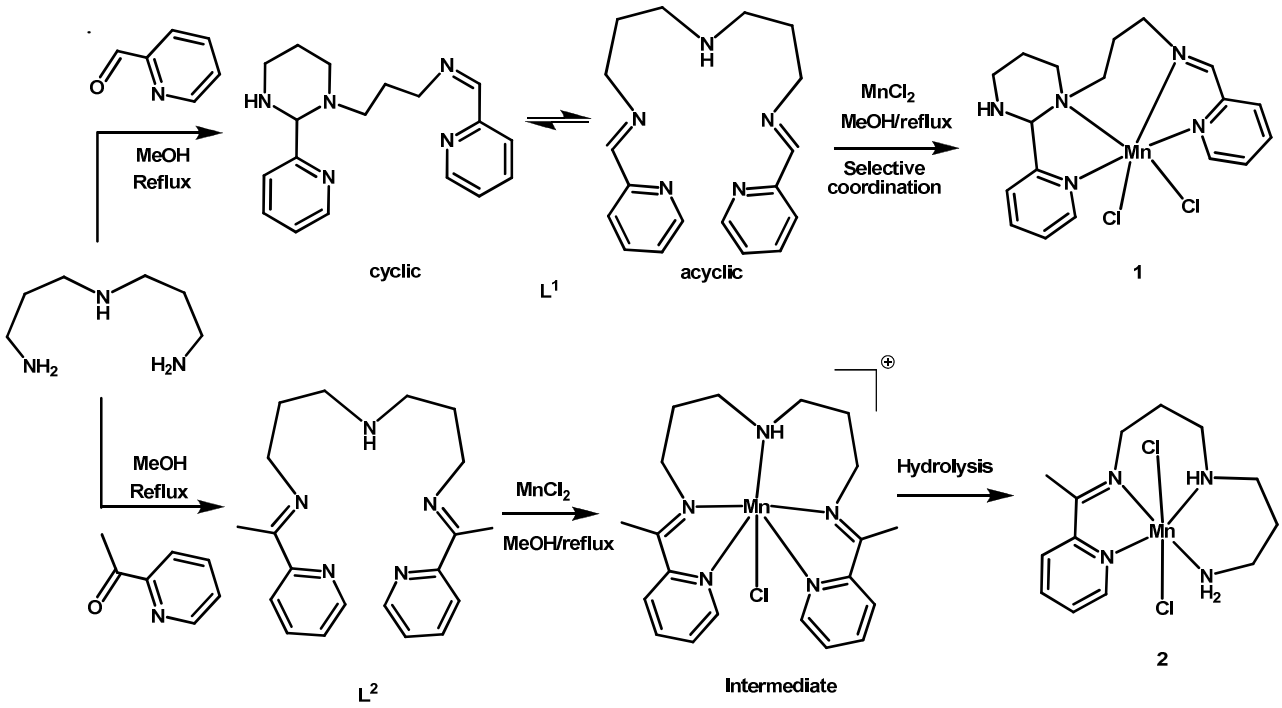

Scheme 1. Synthetic route to complexes **1** and **2**

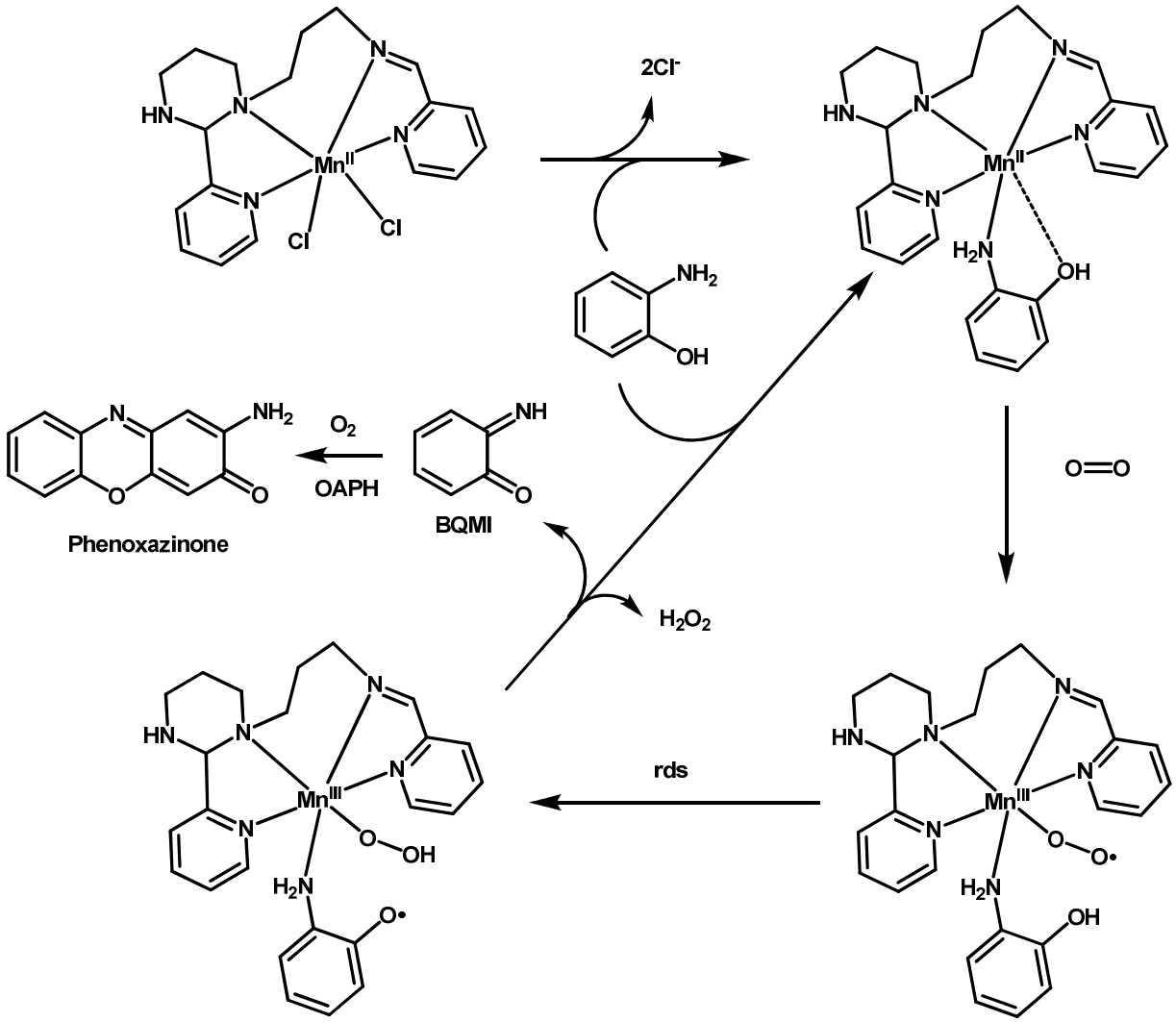

Scheme 2. Plausible mechanistic pathway showing the formation of 2-aminophenoxazine-3-one in which complex **1** chosen as model complex.

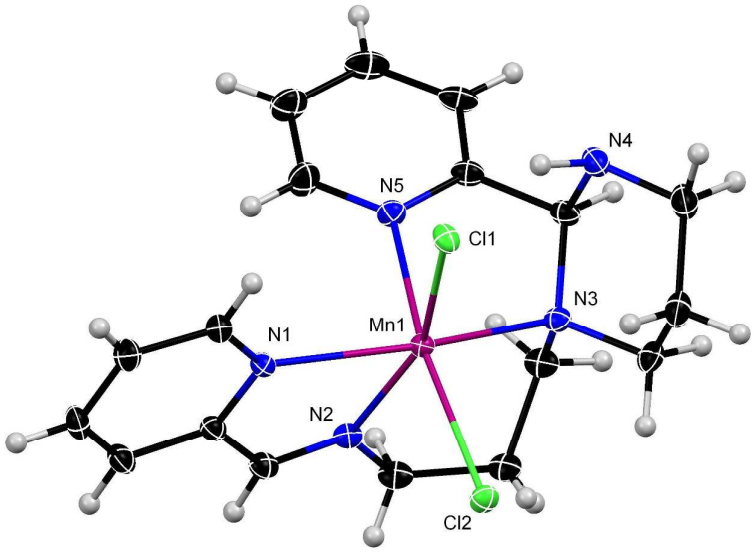

Fig. 1. Crystal structure of $Mn(L^1)Cl_2 \cdot 2MeOH$ (**1**) with the atom labeling scheme. Ellipsoids are drawn at the 50% probability level and solvent molecules are omitted for clarity.

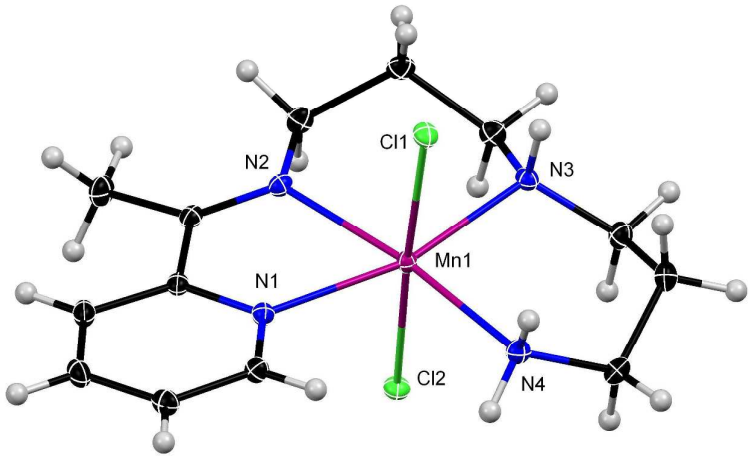

Fig. 2. Molecular structure of $Mn(L^2)Cl_2$ (**2**) with the atom labeling scheme. Ellipsoids are presented at the 50% probability level.

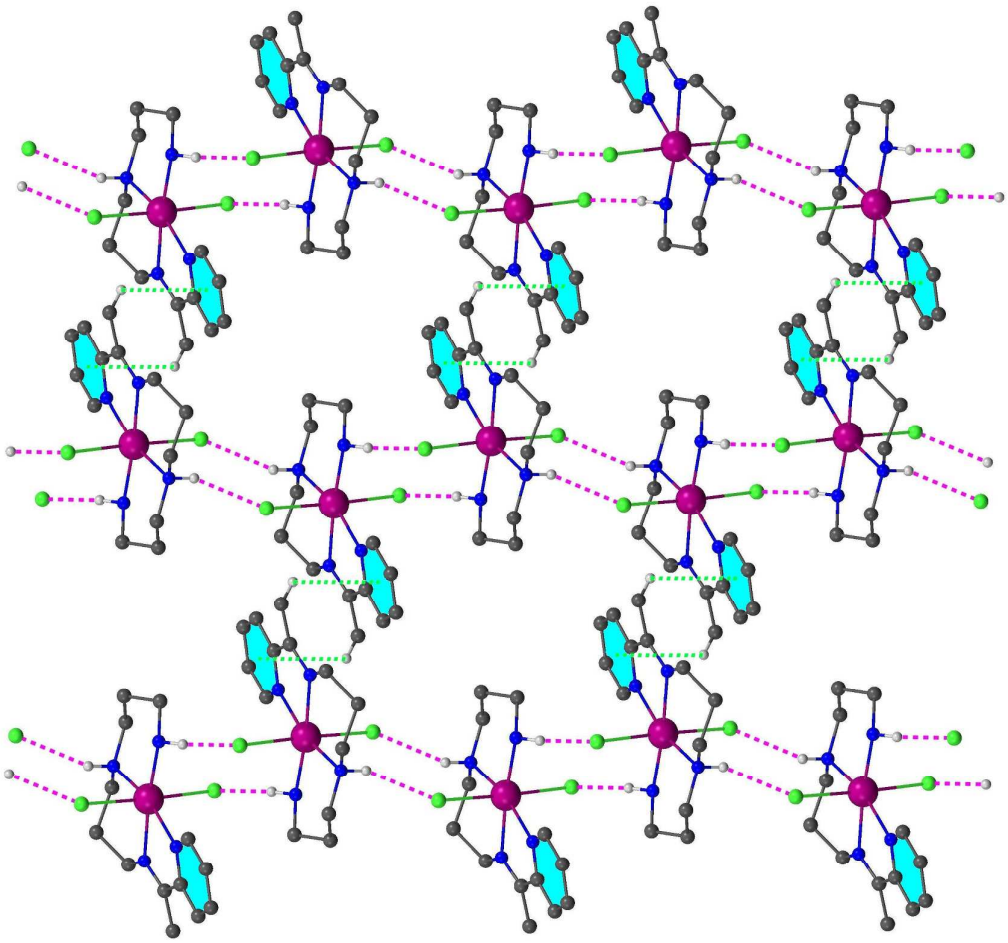

Fig. 3. Molecular packing showing hydrogen bonding and C–H···π interactions in complex **2**; Hydrogen atoms not participating in hydrogen bonding are omitted for clarity

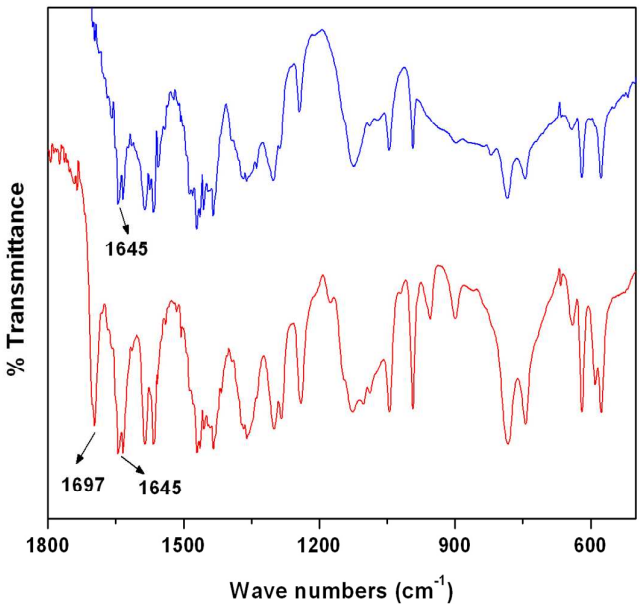

Fig. 4. IR spectra of *in situ* prepared condensation of 3,3′-iminobis(propylamine) and 2-acetylpyridine in 1:2 molar ratio (Top), and upon addition of manganese(II) chloride (Bottom).

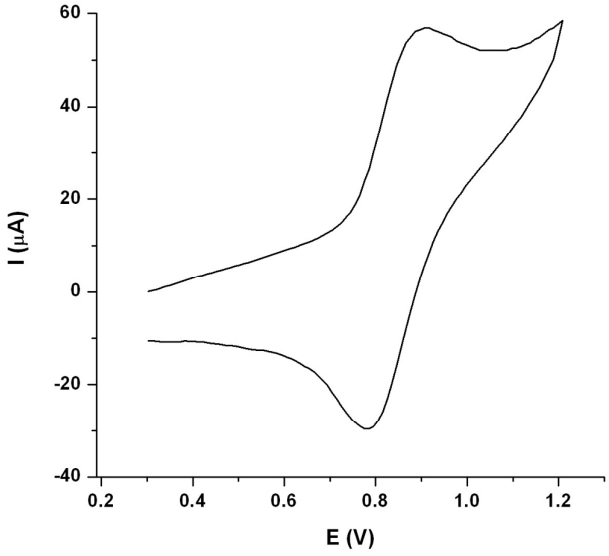

Fig. 5. Cyclic voltammogram of a 5 mM acetonitrile solution of **1** with a conventional three electrode system using a Pt working electrode, Pt auxiliary electrode and Ag/AgCl reference electrode in the presence of tetraethylammonium perchlorate (TEAP) as the supporting electrolyte at ambient temperature; scan rate: 100 mV s^{-1}.

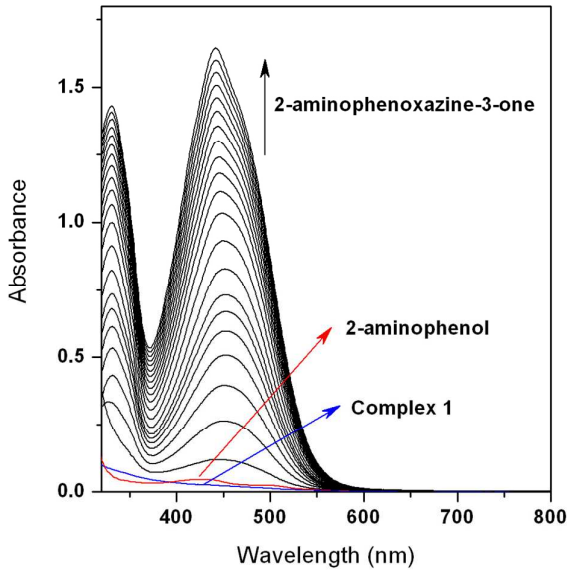

Fig. 6. UV-vis spectral profile showing the growth of phenoxazinone chromophore at 435 nm after the addition of *o*-aminophenol (0.01 M) to a solution of **1** (1 x 10^{-4} M) in methanol at 25 °C. The spectra were recorded for the period of 2 h.

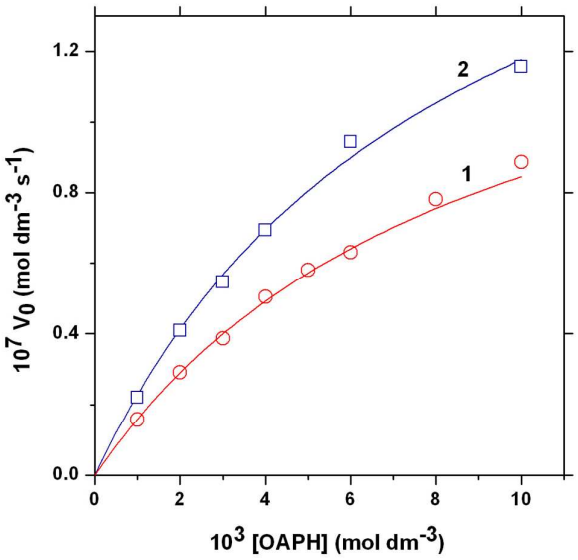

Fig. 7. Initial rate verses substrate concentration plot for the oxidation of *o*-aminophenol catalyzed by **1** and **2** in methanol. Symbols and solid lines represent the experimental and simulated profiles, respectively.

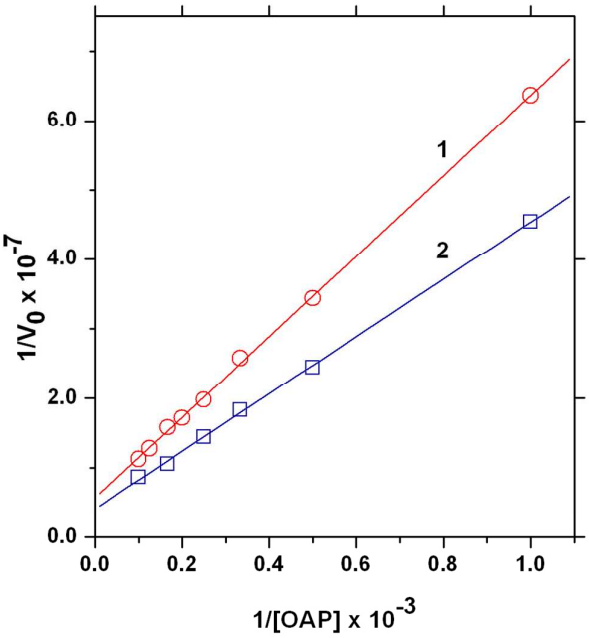

Fig. 8. Lineweaver-Burk plots for the oxidation of *o*-aminophenol catalyzed by **1** and **2** in methanol. Symbols and solid lines represent the experimental and simulated profiles, respectively.